CHARACTERIZATION OF LOCALIZED AND REGIONAL LUNAR PYROCLASTIC DEPOSITS FOR COMPOSITION AND BLOCK POPULATON. D. Trang[1], J. J. Gillis-Davis[1], J. T. S. Cahill[2], B. J. Thomson[3], B. R. Hawke[1], T. A. Giguere[1], P.J. Isaacson[1], D. B. J. Bussey[2], [1]Hawai'i Institute of Geophysics and Planetology, University of Hawai'i at Mānoa, Honolulu, HI, 96822 (dtrang@higp.hawaii.edu) [2]Applied Physics Laboratory, The Johns Hopkins University, Laurel, MD, 20723. [3]Center for Remote Sensing, Boston University, Boston, MA, 02215.

Introduction: Over a hundred individual pyroclastic deposits have been documented [1] and with recent missions, such as the Lunar Reconnaissance Orbiter (LRO), many more have been identified [2]. Earlier works [e.g., 1,3-6] described many of the compositional and physical characteristics that typify localized (<1000 km^2) and regional (>1000km^2) pyroclastic deposits. Mineralogic or chemical compositions were estimated from a few representative VNIR spectra from the pyroclastic deposits [e.g., 4,6]. From these spectra, FeO contents were estimated from the 1-µm absorption band depth and TiO_2 content was predicted from the UV-Vis continuum slope [6]. Later, [7] used radiative transfer theory to determine FeO and TiO_2 content. Other properties explored in past studies include: the crystalline to glass proportions [6], particle size [7], areal coverage [e.g., 1,5,6], and the thickness of the deposits [8]. All of these observations are critical in producing eruptive models [e.g., 4,6,9]. However, to apply these models to the Moon, the location of the vents in regional pyroclastic deposits must also be identified. We distinguish volcanic vents in regional pyroclastic deposits by two methods: (1) analyzing block populations and (2) compositional heterogeneities in each deposit.

Background: In our first method, our goal is to locate volcanic vents based upon block distribution. We use rock abundance as a proxy for vent location because when blocks are transported to the surface during an eruption, the most massive blocks are deposited closest to the vent, whereas less massive blocks are blasted farther from the vent [10]. As an eruption continues, finer pyroclastic material may eventually bury these blocks. However, episodic eruptions may introduce new blocks to the surface of the pyroclastic deposit.

In the second method, our goal is to locate vents on regional pyroclastic deposits based upon the compositional heterogeneities. Regional pyroclastic deposits are suspected to have formed as a result of multiple vents [9]. Our hypothesis is that if the composition of a pyroclastic deposit is spatially heterogenous (assuming no mixing of local surface material), it could indicate two possibilities: (1) That the various compositions are derived from each vent erupting compositionally unique material. (2) A single event has erupted material of more than one composition.

Data & Methods: From the block population perspective, we use localized pyroclastic deposits to develop a surface and subsurface rock abundance model based upon data from the Diviner Lunar Radiometer Experiment [11] and the Miniature Radio-Frequency (Mini-RF) [12]. We investigate the relationship between rock abundance and the properties of the vent in smaller localized deposits first because the vents tend to be conspicuous and usually centered within the deposit. After developing a rock abundance model for localized pyroclastic deposits, we will apply this model into identifying volcanic vents in regional deposits.

We use two daughter product maps from Mini-RF and Diviner. Surface rock abundance (RA) maps, based upon Diviner data, were derived from the anisothermality of the lunar surface [13]. The RA map is sensitive to rocks >1 m in size. We also use S-band (12.6-cm) circular polarization ratio (CPR) maps, as radar is sensitive to both surface and subsurface structures [14]. Radar can penetrate to a depth of about 10-times the wavelength and is sensitive to blocks that are 10^{-1} to 10^{1} times the wavelength collected [15].

In this initial study, we compare complementary RA and CPR products of two localized pyroclastic deposits in Alphonsus W (13.6°S, 4.1°W) and Alphonsus E (14.3°S, 2.0°W) relative to the surrounding area.

As for the compositional perspective, we are developing FeO and TiO_2 maps using the Moon Mineralogy Mapper (M^3). We use M^3 because of its high spectral resolution (85 bands) in the UV-Vis (~0.46-3.0 µm) and high spatial resolution (140 m/px for 100 km lunar polar orbit) [16]. Our plan is to map regions based upon contrasting FeO and TiO_2 content in each deposit. If each volcanic vent is ejecting compositionally unique material, then the center of these regions may be the location of the source.

We construct a FeO and TiO_2 map for pyroclastic deposits by using radiative transfer modeling [i.e., 17,18] with M^3 data. Previous FeO and TiO_2 maps might be inappropriate for pyroclastic deposits because these algorithms assumed that the material is initially crystalline [19]. In contrast to previous work [e.g., 6,7], we employ radiative transfer modeling of M^3 data with optical parameters of synthetic lunar pyroclastic glass [20]. These optical parameters not only models the 1-µm and 2-µm absorptions, but also the two Fe^{2+}-Ti^{4+} intervalence charge transfer (IVCT) bands as well, which may indicate TiO_2 abundance in pyroclastic glass. However, we cannot develop FeO and TiO_2 maps based upon these synthetic glasses because localized pyroclastic deposits contain low abundance of glass [4].

Here, we produce a TiO_2 map of an area in southwestern Humorum (25.9°S, 44.9°W). The area

around this feature was converted to the complex index of refraction (k) and assumed a grain size of 45 µm (based upon approximate grain sizes from Apollo sample 74002 [21]). We performed a spectral match between the optical parameters as a function of FeO and TiO_2 and included an offset and scaling factor to force the model and the data to be within the same magnitude of k.

Results and Future Work: The two localized pyroclastic deposits, Alphonsus W and E, exhibit low surface rock abundance relative to the local environment. For Alphonsus W, we observe a RA increase of 0.001 relative to background. This excludes the vent (which contain rocks probably due to erosion), fresh craters, and rilles. However, in the CPR data, we notice a slight increase in CPR. For Alphonsus W, we observe a CPR increase of 0.01-0.04 relative to background. To better characterize these block populations, we will quantify the rock abundances on the surface and subsurface of other localized pyroclastic deposits.

We provide an example TiO_2 map of the regional pyroclastic deposit in southwestern Humorum (**Fig 2)**. In this map, the mean predicted TiO_2 content is about ~5±2 wt.%. In **Figure 2**, we do not observe any visible changes in TiO_2 content except the northeast corner. This is due to the presence of the maria. Thus, we speculate that a volcanic vent may not be present here.

The spectral range of M^3 may not be able to correctly model the IVCT bands because they reside in the ultraviolet and visible depending on TiO_2 content [20]. Consequently, M^3 is limited to modeling high Ti pyroclastic deposits where the IVCT bands would be apparent within M^3 spectral range. An instrument that can detect this portion of the electromagnetic spectrum is the Lunar Reconnaissance Orbiter Camera (LROC)-Wide Angle Camera (WAC). This imager is sensitive to the ultraviolet and visible bands [22]. Thus, M^3 is preferred for producing FeO maps due to its sensitivity in the near-infrared and the WAC for producing TiO_2 maps because it is sensitive in the UV-Vis.

References: [1] Gaddis et al. (2003), *Icarus*, 161, 262-280. [2] Gustafson et al. (2012), *JGR*, 117, E00H25. [3] Lucey et al. (1986), *JGR*, 91(B4), D344-D354 [4] Hawke et al. (1989), *Proc. 19th LPSC*, 19, 255-268 [5] Gaddis et al. (1985), *Icarus*, 61, 461. [6] Weitz et al. (1998), *JGR*, 103(E10), 22725-22759. [7] Wilcox et al. (2006), *JGR*, 111, E09001. [8] Carter et al. (2009), *JGR*, 114, E11004 [9] Wilson and Head (1981), *JGR*, 86, 2971-3001 [10] Walker et al. (1971), *Geophys. J. R. astr. Soc*., 22, 377-383. [11] Paige et al. (2010), *Space Sci. Rev.*, 150, 125-160. [12] Nozette et al. (2010), *Space Sci. Rev.*, 150, 285-302. [13] Bandfield et al. (2011), *JGR*, 116, E00H02. [14] Carter et al. (2011), *Proc. of the IEEE*, 99(5), 770-782. [15] Ghent et al. (2005), *JGR*, 110, E02005. [16] Pieters et al. (2009), *Curr. Sci*., 96(4), 500-505. [17] Hapke (1981), *JGR*, 86(B4), 3039-3054. [18] Lucey (1998), *JGR*, 103(E1), 1703-1713. [19] Lucey et al. (2000), *JGR*, 105(E8), 20297-20305. [20] Trang et al. (2013), *XLIV LPSC*, 44, Abs #1312. [21] McKay et al. (1978), *Proc. of LPSC*, 9(2), 1913-1932. [22] Robinson et al. (2010), *Space Sci. Rev.*, 150, 81-124.

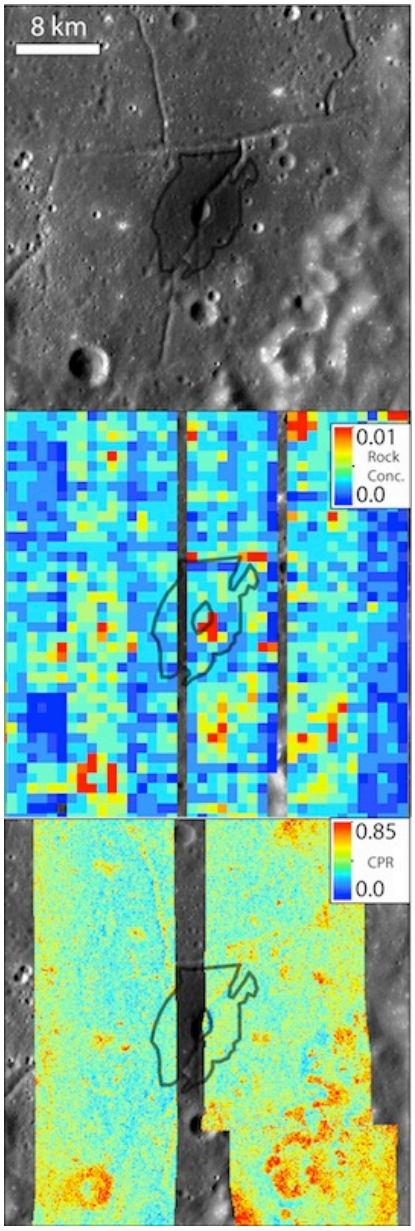

Figure 1: (top) LROC-WAC image: Black outline is the localize pyroclastic deposit of Alphonsus E. (middle) Diviner-derived RA map (middle). (bottom) Mini-RF derived CPR map.

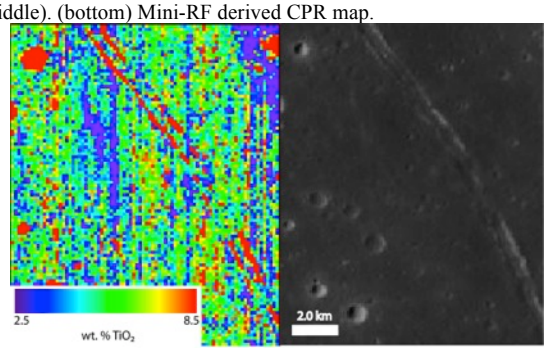

Figure 2: Left is the TiO_2 map of southwestern Humorum. Right is the LROC-WAC image.